

Analysis and design of demountable embedded steel column base connections

Dongxu Li ^{*1}, Brian Uy ^{1a}, Vipul Patel ^{2b} and Farhad Aslani ^{3c}

¹ Centre for Infrastructure Engineering and Safety, School of Civil and Environmental Engineering, The University of New South Wales, Sydney, NSW 2052, Australia

² School of Engineering and Mathematical Sciences, College of Science, Health and Engineering, La Trobe University, PO Box 199, Bendigo, VIC 3552, Australia

³ School of Civil, Environmental and Mining Engineering, The University of Western Australia, Crawley, WA 6009, Australia

(Received September 13, 2016, Revised December 31, 2016, Accepted January 06, 2017)

Abstract. This paper describes the finite element model for predicting the fundamental performance of embedded steel column base connections under monotonic and cyclic loading. Geometric and material nonlinearities were included in the proposed finite element model. Bauschinger and pinching effects were considered in the simulation of embedded column base connections under cyclic loading. The degradation of steel yield strength and accumulation of plastic damage can be well simulated. The accuracy of the finite element model is examined by comparing the predicted results with independent experimental dataset. It is demonstrated that the finite element model accurately predicts the behaviour and failure models of the embedded steel column base connections. The finite element model is extended to carry out evaluations and parametric studies. The investigated parameters include column embedded length, concrete strength, axial load and base plate thickness. Moreover, analytical models for predicting the initial stiffness and bending moment strength of the embedded column base connection were developed. The comparison between results from analytical models and those from experiments and finite element analysis proved the developed analytical model was accurate and conservative for design purposes.

Keywords: embedded column base connections; monotonic and cyclic loading; demountability; finite element analysis; analytical model

1. Introduction

In recent years, attempting to design structures more sustainably and being made demountable is gaining popularity in the construction industry. This trend is mainly driven by two factors. Firstly, the construction industry has significant negative impacts on the environment. As indicated, the production and transportation of construction components contributed significantly to the greenhouse gas emissions (Lorenz and Vangeem 2011). The Green Building Council of Australia (2009) reported that a large amount of landfill waste can also be attributed to the disposal of construction and demolition waste. Secondly, many structures and components have to be adapted, relocated or repaired to meet the needs of the new owners. In order to fulfill the concept of designing structures being demountable, structural steel was one of the most ideal construction materials, since it can be reused multiple times without the loss of material properties (Winters-Downey 2010).

Steel column base connection could have a considerable influences on the behaviour and performance of the steel moment resisting frames, which are generally utilised in seismic-prone regions. Steel column base connection is normally classified as an exposed bolted system, socket system and embedded system (Fig. 1). Exposed bolted steel column base connections have been popularly used in low-to medium-rise steel structures due to their improved constructability (Grauvilardell *et al.* 2005, Cui *et al.* 2009). For mid- to high-rise steel moment resisting frames, steel column base connections are often designed with socket and embedded systems, where steel columns are embedded into the high strength mortar or concrete foundation to achieve a stiffer constraint and better performance in the cyclic condition (Grilli and Kanvinde 2015). Koch *et al.* (1993) conducted an experimental study on 72 embedded column base connections subjected to bending moment and shear force. An improved design concept was proposed and it was found that the lengths of embedment of the steel columns can be reduced. Pertold *et al.* (2000) tested two different types of experimental specimens under axial loading and calibrated a numerical model with test results. An analytical model for the embedded steel column base was also developed for the prediction of bending moment, shear and axial capacity. Cui *et al.* (2009) performed a series of tests on shallow embedded steel column base connections under horizontal cyclic loading to very large deformations. By analysing a few variables, it was found to be practical to

*Corresponding author, Ph.D. Student,
E-mail: d.li@unsw.edu.au

^a Professor, E-mail: b.uy@unsw.edu.au

^b Lecturer, E-mail: v.patel@latrobe.edu.au

^c Senior Lecturer, E-mail: farhad.aslani@uwa.edu.au

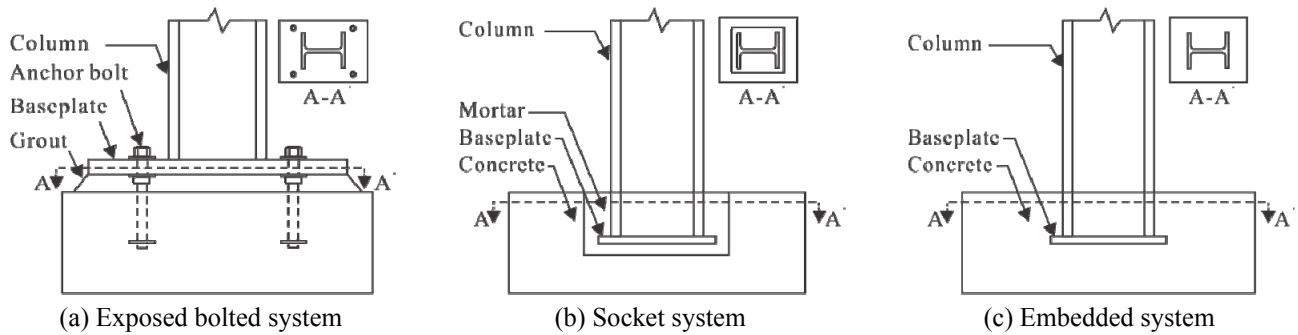


Fig. 1 Typical steel column base connections

strengthen the shallow embedded column base connections so that it could behave like a fully embedded column base. Heristchian *et al.* (2014) presents the test results of the pullout failure of three embedded steel column base connections. As concluded, the steel columns, which was embedded into concrete foundations without anchor bolts can achieve the required resistance against pullout forces. Demir *et al.* (2014) tested four series of embedded steel column base connections under cyclic loading with different design details. It was found that the connection, which was embedded into the concrete foundation performs better than that embedded into high strength mortar. Grilli and Kanvinde (2015) reported experimental results of five embedded column base connections under cyclic loading. The authors developed design models to determine the moment capacity of the embedded column base connection.

The above literature review demonstrates that accurate finite element model for embedded steel column base connections under cyclic loading has not been developed yet. Moreover, the studies on the analytical models to predict the moment capacity and initial stiffness of the embedded steel column base connection were limited. Furthermore, studies on demountability of connections have not been conducted. The concept of demountable connections was presented by Uy (2014) and Uy *et al.* (2016), who suggested that the steel column and connections could deform elastically without undergoing large plastic deformations, which results in the reuse of steel columns after their useful service life. This paper presents finite element models using ABAQUS (2012) for predicting the behaviour and demountability of embedded steel column base connections under monotonic and cyclic loading. In addition, the fixity and moment capacity of embedded column base connections effect the building performance and accurate estimation results in safer and cost effective design in engineering practice. In this paper, analytical models for predicting the initial stiffness and bending moment capacity were proposed. The results from analytical models were further compared with those from experimental programs and finite element analysis.

2. Finite element model

2.1 Basic concept

Full-scale tests can be used to obtain the most reliable behaviour of embedded steel column base connections,

however, they are time consuming and expensive to examine the effects of every parameter. To propose a procedure for the design of the embedded steel column base connection, limited experimental data is insufficient. The finite element analysis program ABAQUS (2012) is employed herein for the nonlinear analysis of embedded steel column base connections.

2.2 Mesh, interactions, boundary conditions and loading

A typical finite element model of an embedded column base connection is depicted in Fig. 2, in which steel column, base plate and concrete foundation were modelled with three-dimensional solid elements. In particular, 8-node linear brick elements with reduced integration (C3D8R) were utilised to simulate the steel column, base plate and concrete foundation to reduce the computational time (Mirza and Uy 2011). A 2-node linear three-dimensional truss element (T3D2) was employed for simulating the reinforcement.

Appropriate mesh size ensures the accuracy and efficiency of the finite element model. In this paper, a mesh sensitivity analysis was performed to provide a rational mesh size for each modelling part. Based on the sensitivity analysis, the mesh size of the column and base plate was determined to be $L/30$ and $B_p/20$, in which L and B_p represent the column height and width of the base plate. The concrete foundation has a limited effect on the analysis results; therefore, a relative coarser mesh size was determined as $B_c/15$, which B_c representing the width of the concrete foundation.

For the embedded steel column base connection, the surfaces coming into contact are the outer surfaces of

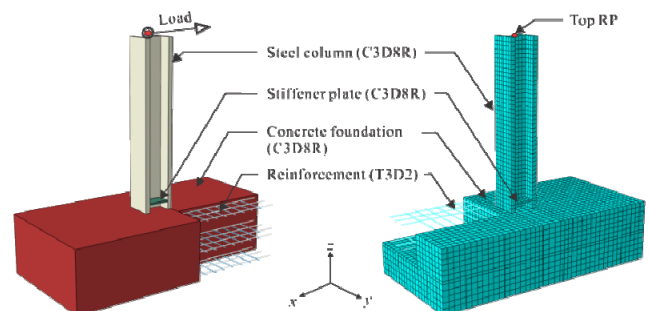


Fig. 2 Finite element model for embedded steel column base connections

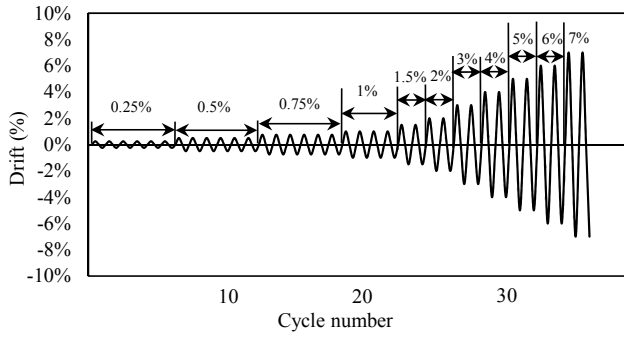


Fig. 3 SAC loading protocol for steel structures in cyclic loads

steel columns and base plates to the surfaces of the surrounding concrete foundations. To accurately predict the behaviour of the embedded steel column base connection, “surface-to- surface” contact with a Hard Contact model in the normal direction and a Coulomb Friction model in the tangential direction was utilised. As suggested by Eurocode 3 (2005), a friction coefficient between steel-to-concrete component was assigned as 0.6. Moreover, “Embedded” constraint was utilised to simulate interactions between the reinforcement and the surrounding concrete.

The bottom ends of the embedded steel column base connections were constrained with fix-ended boundary conditions. All nodes on the top surface of the steel column were tied with a centrally located reference point. The axial loads and horizontal deformation were applied to the top reference point. In particular, the SAC cyclic loading history (Clark *et al.* 1997) with 36 cycles was applied in the horizontal direction of the top reference point, as shown in Fig. 3. SAC cyclic loading history is one of the formal protocols developed for seismic evaluation of steel structures.

2.3 Material models

2.3.1 Concrete in monotonic loading

A damage plasticity model defined in ABAQUS was used to simulate the concrete behaviour in compression and tension. Under monotonic loading, concrete material parameters required to be defined include elastic modulus (E_c), Poisson’s ratio (ν_c), flow potential eccentricity (e), viscosity parameter (μ), dilation angle (ψ), shape factor for yield surface (K_c), the ratio of initial equibiaxial compressive yield stress to initial uniaxial compressive yield stress (f_{b0}/f_c). As suggested by ACI (2008), Poisson’s ratio was adopted as 0.2 and the elastic modulus of the concrete was determined from $E_c = 3320f_c^{0.5} + 6900$, where f_c is in MPa. Flow potential eccentricity (e) is taken as 0.1 and viscosity parameter is determined to be 0.001. Suggested by Aslani *et al.* (2015), 40° is normally used for dilation angle (ψ), f_{b0}/f_c equals to $1.5(f_c)^{-0.075}$ and $K_c = 5.5/[5+2(f_c)^{0.075}]$.

Equivalent stress-strain relationships of concrete in compression and tension are shown in Fig. 4(a). The formula proposed by Carreira and Chu (1985) was adopted to represent the compressive stress-strain curve of concrete. The concrete stress in compression is assumed to be linear

up to a value of $0.4f_c$. Beyond this point, the stress is represented as a function of strain

$$\sigma_c = \frac{f_c \gamma (\varepsilon_c / \varepsilon'_c)}{\gamma - 1 + (\varepsilon_c / \varepsilon'_c)^\gamma} \quad (1)$$

where $\gamma = |f_c / 32.4|^3 + 1.55$ and $\varepsilon'_c = 0.002$. The tensile behaviour of concrete is assumed to be linear until the uniaxial tensile stress is reached, where concrete cracks. The concrete uniaxial tensile stress is taken as $0.56(f_c)^{0.5}$. Beyond this failure stress, the tensile stress linearly reduces to zero with respect to strain.

2.3.2 Concrete in cyclic loading

To simulate the concrete behaviour in cyclic loading, damage mechanics material constitutive laws were used. In this analysis, unilateral damage law with two damage variables (d_t and d_c) is included to describe the concrete behaviour. The concrete damage in tension and compression is denoted with d_t and d_c , respectively. Fig. 4(b) exhibits the concrete behaviour in cyclic loading. Initially, the concrete behaves linearly up to the tensile failure stress f_t . Beyond this stress, the concrete behaviour is defined by a post failure stress-strain relationship modeled by “Tension Damage” (Ali *et al.* 2013, Thai and Uy 2015). During the transition of load from tension to compression, the elastic stiffness of concrete is damaged as the unloading response starts to weaken. Similarly, the “Compression Damage” model is utilised when the loading is reversed from compression to tension. The concrete elastic stiffness degradation can be characterised by the tension damage variable (d_t) and compression damage variable (d_c), as shown in Eqs. (2)-(3)

$$E_t = (1 - d_t)E_0 \quad (2)$$

$$E_c = (1 - d_c)E_0 \quad (3)$$

in which, the concrete damage variables are determined through Eqs. (4)-(7)

$$d_c = 1 - \frac{\sigma_c / E_0}{\varepsilon_{c,pl} (1/b_c - 1) + \sigma_c / E_0} \quad (4)$$

$$d_t = 1 - \frac{\sigma_t / E_0}{\varepsilon_{t,pl} (1/b_t - 1) + \sigma_t / E_0} \quad (5)$$

where $b_c = \varepsilon_{c,pl} / \varepsilon_{c,in}$ and $b_t = \varepsilon_{t,pl} / \varepsilon_{t,ck}$. As suggested by Birtel and Mark (2006), b_c and b_t were taken as 0.7 and 0.1, respectively. Moreover, $\varepsilon_{c,pl}$ and $\varepsilon_{t,pl}$ are the equivalent plastic strains; $\varepsilon_{c,in}$ and $\varepsilon_{t,ck}$ represent the concrete inelastic and cracking strain in compression and tension, respectively.

$$\varepsilon_{c,in} = \varepsilon_c - \sigma_c / E_0 \quad \varepsilon_{t,ck} = \varepsilon_t - \sigma_t / E_0 \quad (6)$$

In addition, recovery factors w_t and w_c in Fig. 4(b), were used to determine the tensile and compressive stiffness recovery. In this analysis, it is assumed that the concrete can

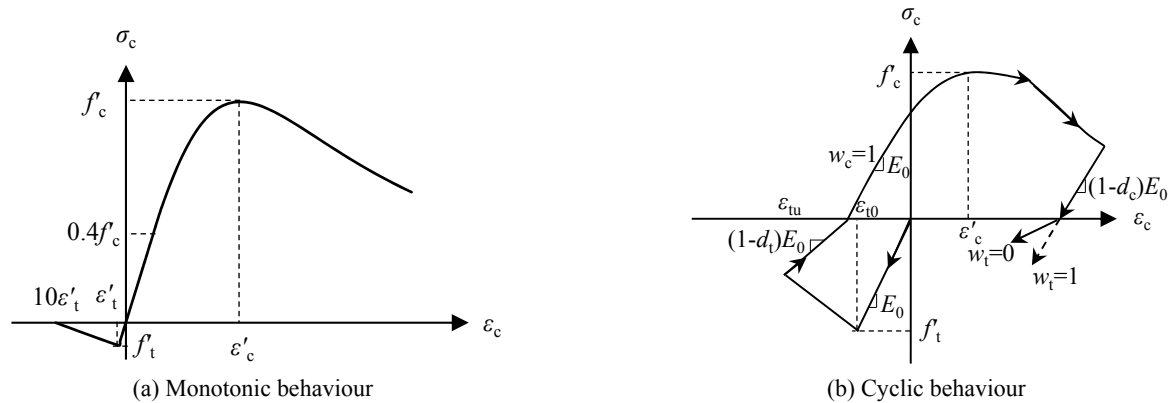


Fig. 4 Stress-strain relationship for concrete

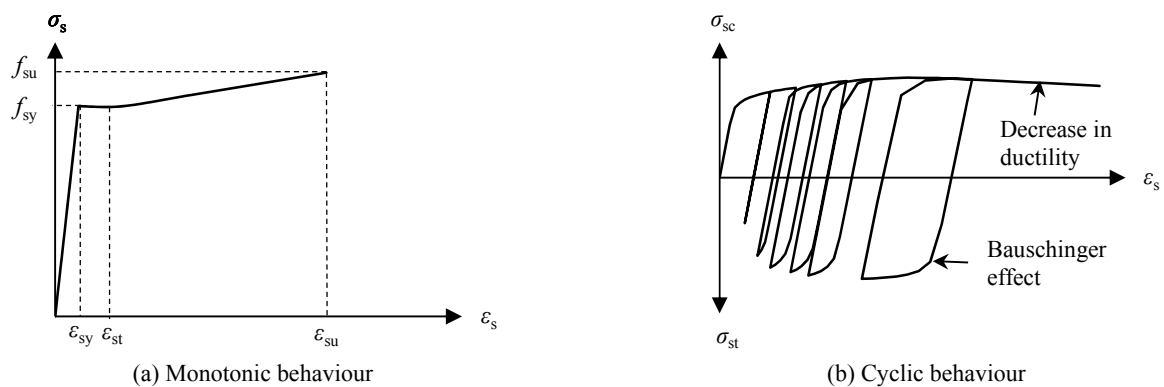


Fig. 5 Stress-strain relationship for structural steel

regain full stiffness with no damage and compressive recovery variable (w_c) was taken as 1. However, no tensile stiffness was assumed to recover and tensile recovery variable (w_t) was determined to be 0.

2.3.3 Structural steel in monotonic loading

The stress-strain relationships of steel column and base plate are essentially similar. Their behaviour is initially elastic after which yielding and strain hardening develop. In the present study, a typical tri-linear stress-strain curve was utilised for simulating the behaviour of structural steel as shown in Fig. 5(a). The three stage material constitutive model considers that the steel exhibits the same stress and strain in compression and tension. In Fig. 5(a), σ_s represents the steel stress, ϵ_s denotes the steel strain, f_{sy} is the yield stress of the steel, ϵ_{sy} represents the yield strain of the steel, ϵ_{st} is the strain at which strain hardening commences (taken as 0.005), ϵ_{su} is the ultimate strain and f_{su} is the ultimate tensile stress of the steel.

2.3.4 Structural steel in cyclic loading

The performance of structural steel under cyclic loading has been seen to be different from that in monotonic condition (Jia and Kuwamura 2014, Silvestre *et al.* 2015). Due to the Bauschinger effect, reversed yield stress was decreased and the hardening behaviour is strongly affected by the previous strain history. In this analysis, the complex three-component nonlinear kinematic rule and combined with isotropic hardening model was developed based on

Chaboche's (1994) model, through which Bauschinger effect, pinching effect and ratcheting response can be well predicted. For this combined hardening model, the parameters need to be determined and can be categorised into isotropic and kinematic parameters. In particular, σ_0 is the yield stress at zero plastic strain.

Q represents the maximum change in the size of the yield surface and b is the rate at which the yield stress change with plastic strain. These isotropic parameters dominate the shape of the yield surface of the steel element under cyclic loading. For kinematic behaviour, C_1 to C_3 are the kinematic hardening modulus and γ_1 to γ_3 represent the rate at which hardening modulus decrease with plastic strain. Fig. 5(b) illustrates an example of the stress-strain relationship of structural steel in cyclic loading. As observed from the Fig. 5(b), the hardening behaviour of structural steel is affected by the previous strain accumulation. The damage accumulation ensures the decrease of yield stresses in the reversed cycles.

2.4 Verification of finite element models

In this study, four experimental specimens with various design details conducted by Koch *et al.* (1993) and Grilli and Kanvinde (2015), were selected to evaluate the reliability of the developed finite element model. The geometry and material details are given in Table 1.

The validation of the finite element model for the embedded column base connections under monotonic

Table 1 Geometric and material property details for validated specimens

Specimen	Axial load P (kN)	Embed length L_{Emb} (mm)	Steel column	Base plate dimension ($B_p \times D_p \times t_p$) (mm)	Concrete strength f'_c (MPa)	Ref.
Test 6	0	1000	HEB 200	-	65	Koch <i>et al.</i> (1993)
Test 26	0	600	IPE 600	-	34	
Test 2	445	508	W18×311	864×711×51	30	Grilli and Kanvinde (2015)
Test 3	0	762	W14×370	762×762×51	30	

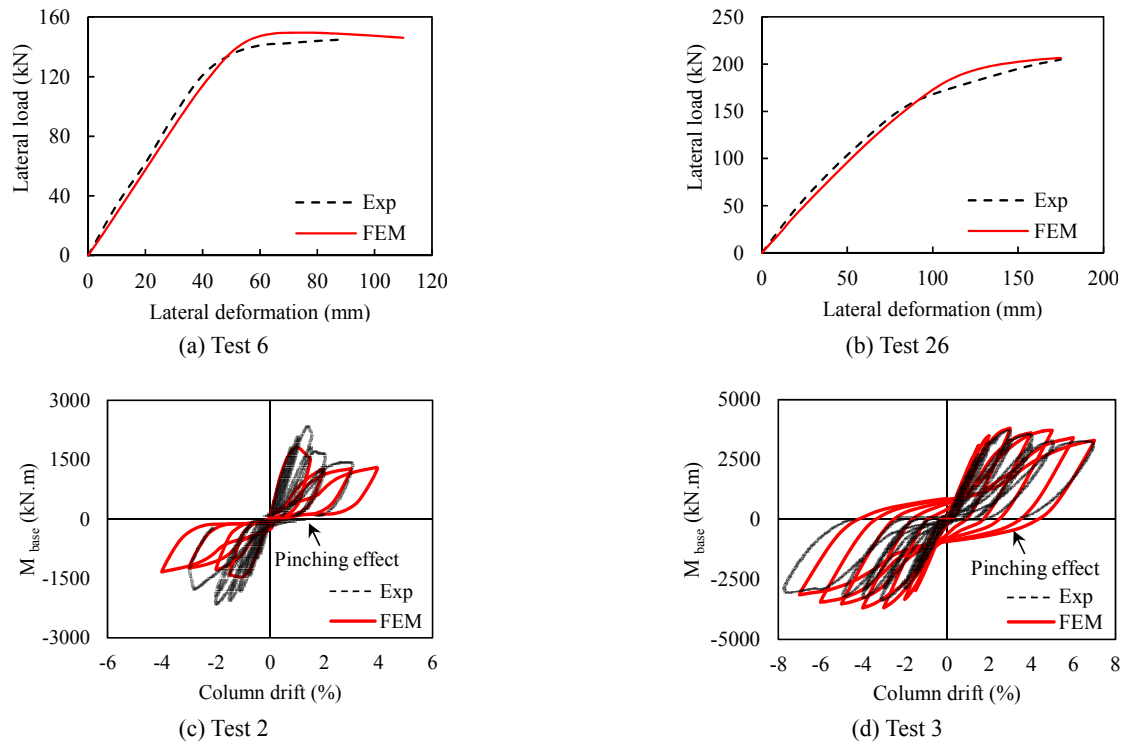


Fig. 6 Validation of finite element models for various specimens

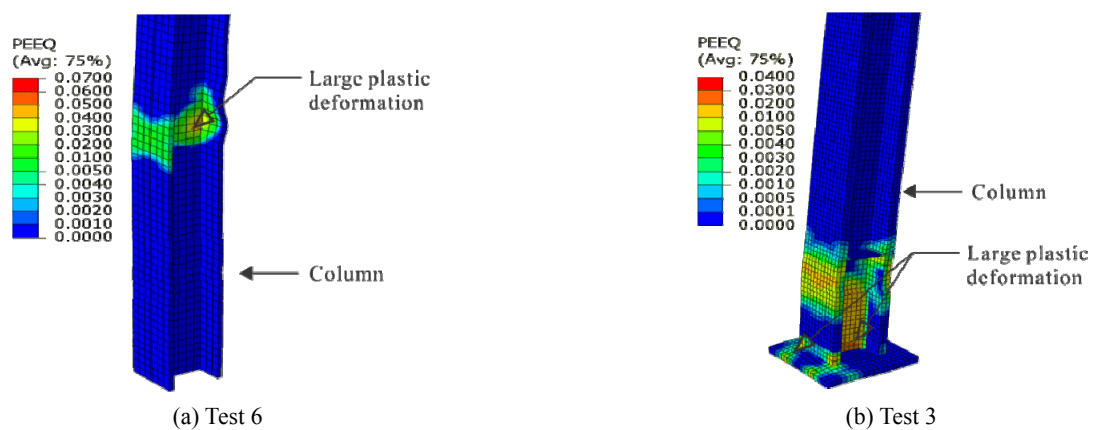


Fig. 7 Large plastic deformation in embedded steel column base connection

loading is presented in Figs. 6(a) and (b). As can be seen, the finite element model can accurately predict the initial stiffness and bending moment capacity of the embedded steel column base connection. The finite element model is slightly conservative in terms of initial stiffness prediction. In addition, the finite element model over-predicts the

bending moment capacity of the embedded column base connection by 1.5%. And the deviation in the plastic region between finite element analysis and experimental results may be attributed to the use of the idealised stress-strain relationship for structural steel. Figs. 6(c) and (d) illustrate the validation of finite element model for embedded column

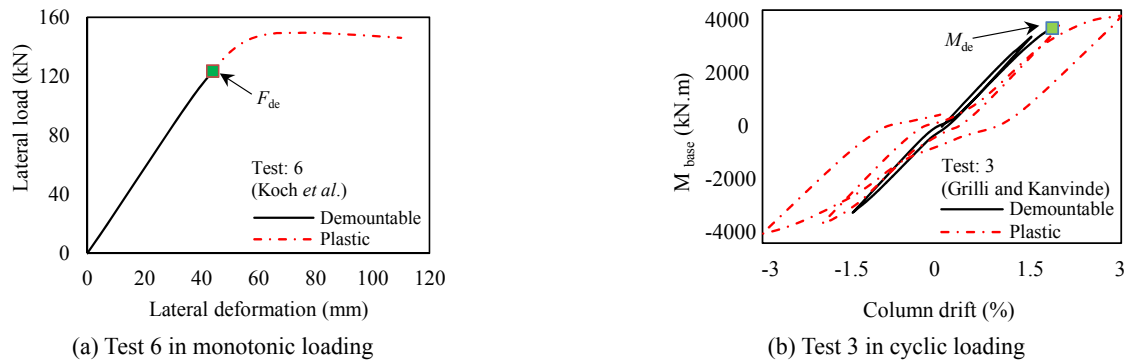


Fig. 8 Demountability of embedded steel column base connections

base connections under cyclic loading. As shown in the Fig. 6, the developed finite element predictions agree well with the experimental results. The pinching effects and the accumulation of strain damage can be well simulated.

Overall, the results obtained from the finite element model agree well with the experimental data, and the slight deviation in the post-yield region does not affect the accuracy of the finite element model since demountable connections only need to be simulated in the elastic region.

3. Demountability and plastic damage

Embedded steel column base connections can be dismantled at the end of their service life by crushing the concrete foundations with specific tools. Since no reinforcement or concrete are casted between the steel column flanges, the connections can be easily dismantled. Moreover, the study presented herein is mainly focused on the demountability analysis of the embedded steel column base connection with traditional design details.

Uy *et al.* (2015, 2016) indicated that elasticity of a steel component is characterised by the ability to sustain elastic deformation without undergoing significant plastic deformation. Fig. 7 depicts typical failure modes for embedded steel column base connections. As can be seen, large plastic deformation occurred in the column and base plate of the connections. When considering the demountability of embedded steel column base connection, large plastic deformation occurred in the column and base plate will be accounted. PEEQ in Fig. 7 represents a zero equivalent plastic strain, which can be regarded as the yield strain of the steel members. Steel members are reusable providing no large plastic deformation occurred, which can be achieved when steel members' PEEQs are smaller than their yield strains.

For the purposes of introducing the concepts of demountability of embedded steel column base connection, Tests 6 and 3 in Table 1 were utilised as examples and the predicted lateral load-deformation curve and moment-column drift curve based on finite element models are illustrated in Fig. 8. It can be observed from Figs. 8(a) and (b) that when the PEEQ is predicted to be less than the yield strain, the connections can be demounted up to 124 kN and 3370 kN.m, respectively. Specifically, the loading and

Table 2 Details of parametric studies

Parameters	Values		
*Embedded length L_e/D_{col}	1.0	1.5	2.0
*Concrete strength f_c (MPa)	20	30	50
*Axial load P (kN)	10% P_{des}	20% P_{des}	40% P_{des}
**Base plate thickness t_{bp} (mm)	25	50	75

* Effects of embedded length, concrete strength and axial load are investigated for both design details;

** Effects of base plate thickness are investigated for Design 2 only

unloading paths of Test 3 in the first 23 cycles coincide, which indicates that the embedded column base connection behaves elastically when horizontal cyclic deformation is small. In the 24th cycle, which is the start of intermediate seismic level, large plastic deformation was observed in the column web, which results in the demountability of the connection being difficult to achieve.

F_{de} and M_{de} shown in the figures represent the force and moment where large plastic deformation in the connection occurred. The curve beyond this point indicates large plastic deformation was observed in the steel members. Therefore, F_{de} and M_{de} is the maximum force and bending moment, at which the steel column and base plate are demountable and reusable.

4. Parametric study

This section presents and discusses the results of parametric analysis on the embedded column base connections using the developed finite element models. The most commonly used design for embedded column base connections (Design 1 and 2) are illustrated in Fig. 9. In this analysis, parametric study of the main variables for embedded column base connection was carried out to examine their potential effects. The authors herein take into account four different variables as shown in Table 2. In particular, effects of embedded length, axial load and concrete strength were investigated for connections with both design details; while the effects of the base plate thickness were studied for connections of Design 2 only. Moreover, the effects of the aforementioned variables on the demountability of the connections were studied.

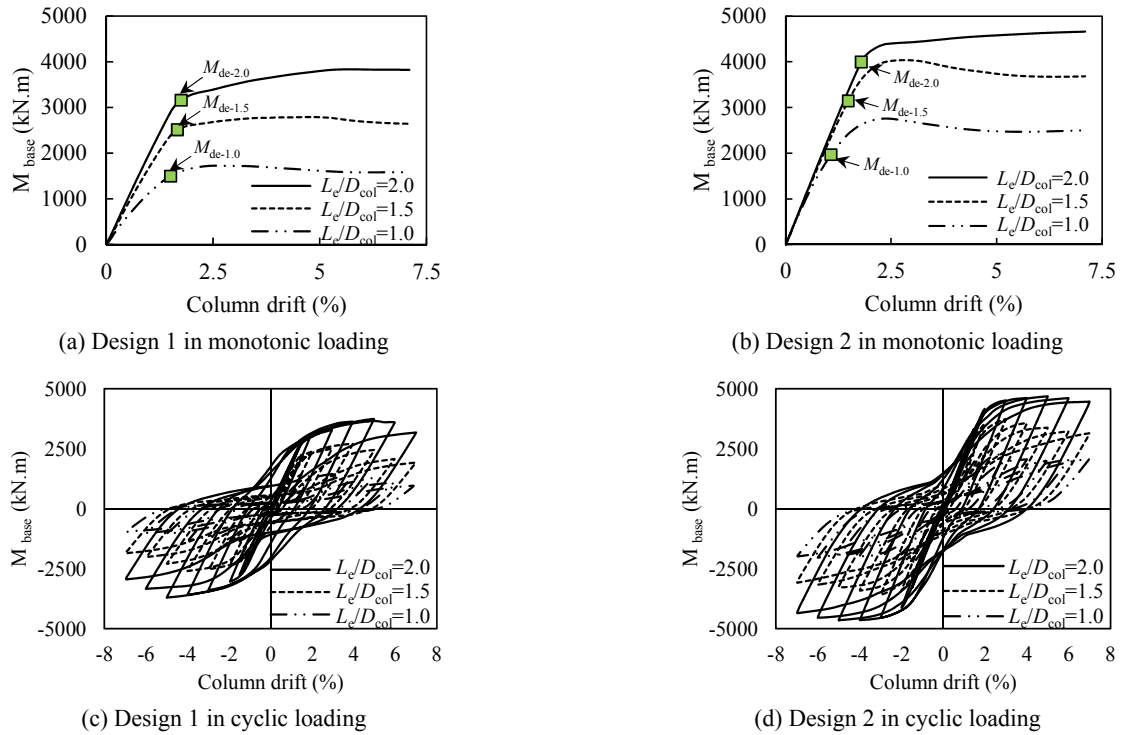


Fig. 10 Effects of embedded length on moment-column drift curves

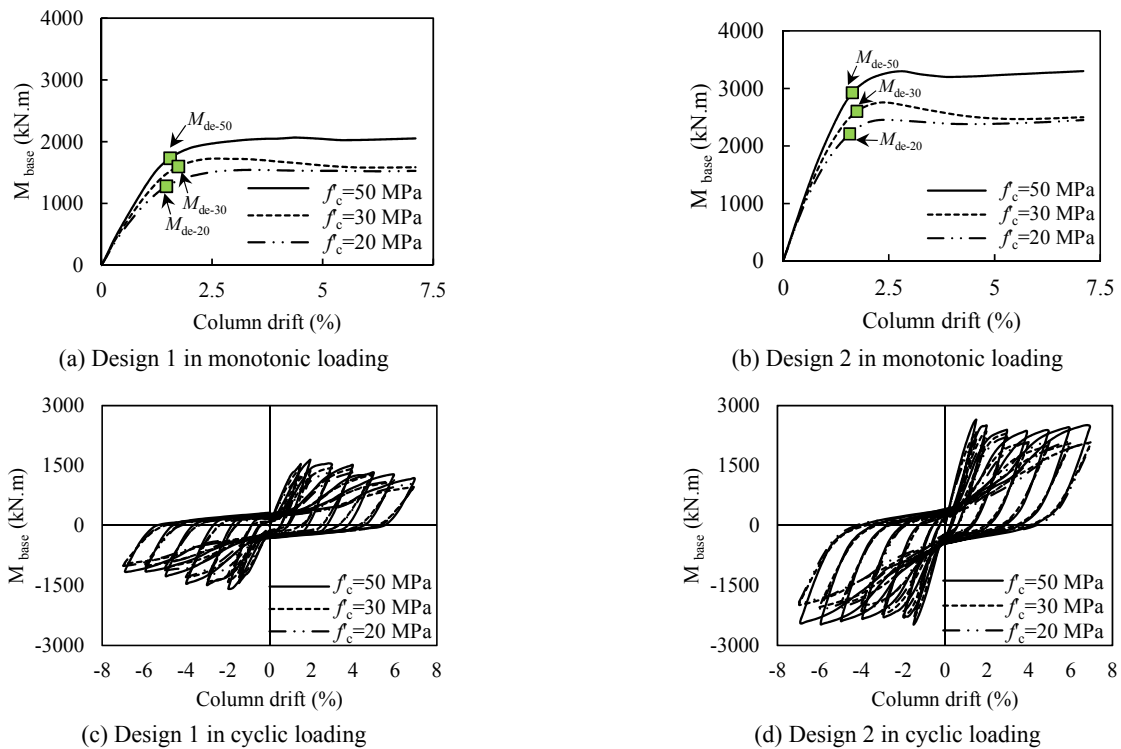


Fig. 11 Effects of concrete strength on moment-column drift curves

4.1 Effects of embedded length L_e/D_{col}

Three different embedded lengths were used in the parametric studies which included $L_e/D_{col} = 1, 1.5$ and 2 . It should be noted here that the concrete foundation was assumed to be large enough, which means in this analysis,

the punching failure of the concrete foundation was not included. The investigated focus is the steel member with flexural failure. The moment-column drift curves for connections with Design 1 (Fig. 10(a)) showed that increasing the embedded length of the steel column increases the initial stiffness and bending moment capacity

of the connection. In particular, bending moment was increased by 62% and 122% when increasing the embedded length from $L_e/D_{col} = 1$ to $L_e/D_{col} = 1.5$ and 2, respectively. Fig. 10(b) compared the moment-column drift curves with different embedded lengths for connections of Design 2. It was found that the embedded length had similar effects. In addition, with the same embedded length, the initial stiffness and moment capacity for the connections of Design 2 was higher than that from connections of Design 1. Figs. 10(c) and (d) illustrate the effects of the embedded length on the cyclic behaviour of embedded column base connections. Conclusions from finite element analysis are similar to those in monotonic loading, initial stiffness and bending moment were significantly increased by increasing the embedded length.

The demountability of the embedded column base connections were significantly affected by the column embedded length, shown in Figs. 10(a) and (b). For connections of Design 1, M_{de} was increased by 65% and 104% when increasing the embedded length from $L_e/D_{col} = 1$ to $L_e/D_{col} = 1.5$ and 2, respectively.

4.2. Effects of concrete strength f_c

Three different concrete strengths (20, 30 and 50 MPa) were used in the parametric studies to examine the influences of concrete strength on the moment-column drift curves. Figs. 11(a) and (b) show a comparison of the moment-column drift curves with a difference in concrete strength under monotonic loading for both design details. As can be seen, the increase in concrete strength results in higher initial stiffness and bending moment capacity. Figs. 11(c) and (d) presents the results for embedded column base

connections under cyclic loading. Similar to monotonic loading, the initial stiffness and bending moment capacity were increased with the increase in concrete strength. However, the ductility of the embedded column base connection is lowered by increasing the concrete strength.

Figs. 11(a) and (b) also illustrate the effects of concrete strength on the demountability of the embedded column base connections with different design details. The use of higher concrete strength leads to a higher demountable bending moment (M_{de}). In addition, the effects of higher concrete strength on the demountability for connections of Design 2 are more significant than that for connections of Design 1.

4.3. Effects of axial load P

To study the effect of axial load, the finite element analysis with 10%, 20% and 40% of the design compressive capacity of the column (P_{des}) was conducted. As observed in Fig. 12(a), the increase in axial load increases the initial stiffness and moment capacity of the embedded column base connection. For connections of Design 2 (Fig. 12(b)), there is no significant change in initial stiffness induced by increasing axial load. Moment capacity was increased by 7.5% when increasing axial load from 10% P_{des} to 20% P_{des} . However, the moment capacity decreased significantly by 15% when increasing axial load from 20% P_{des} to 40% P_{des} . This reduction in bending moment capacity is due to the occurrence of local buckling in the steel column. Again, both the initial stiffness and bending moment capacity for embedded column base connections of Design 2 are higher than that from connections of Design 1. Figs. 12(c) and (d) present the results for embedded column base connections

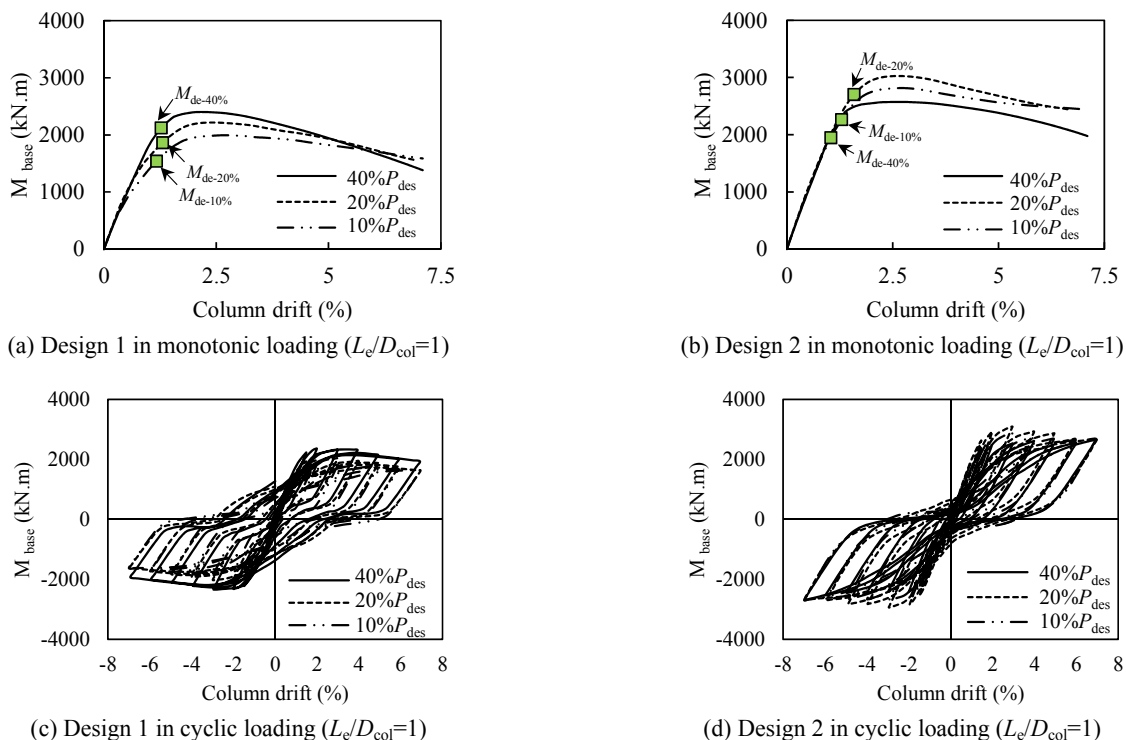


Fig. 12 Effects of axial load on moment-column drift curves

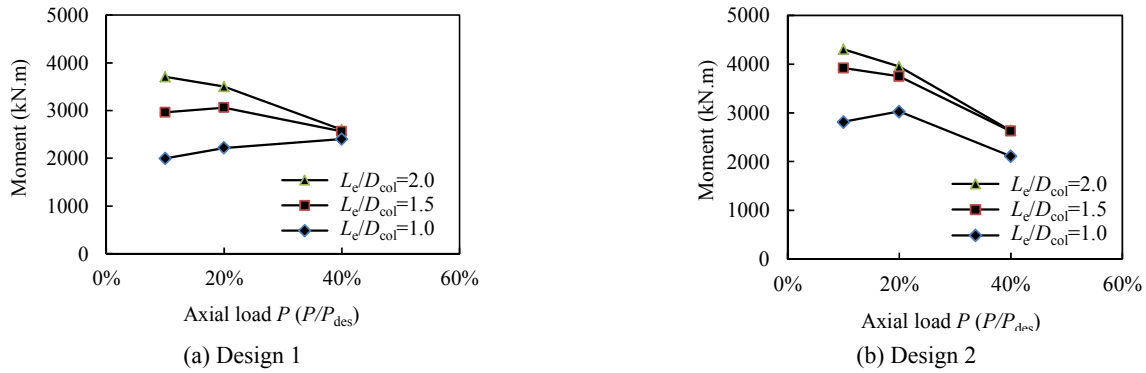


Fig. 13 Effects of axial load on moment-column drift curves with different embedded lengths

under cyclic loading. Finite element analysis results were found to be similar to those under monotonic loading. Higher axial load increases the moment capacity and initial stiffness for connection of Design 1, while higher axial load results in the local buckling of steel column for connections of Design 2.

Effects of axial load on the demountability for the embedded column base connections were investigated and presented in Figs. 12(a) and (b). For the embedded column base connections without base plates (Design 1), the demountability of the column can be increased with an increase in the axial load. However, the demountability was significantly reduced when increasing axial load to 40% P_{des} , where the local buckling of the steel column was observed.

The analysis results shown in Fig. 12 are from the connections with an embedded length of $L_e/D_{col} = 1$. Varying the column embedded length, the effects of axial load are different, which is shown in Fig. 13. As can be seen in Fig. 13, the higher axial load shifted the failure mode of embedded steel column base connection from the concrete crushing of the foundation to the buckling of steel column.

4.4 Effects of base plate thickness t_{bp}

Fig. 14(a) depicts the comparison of the moment-column drift curves with different base plate thicknesses. It can be observed that the moment capacity and ductility would increase with an increase in base plate thickness, which is to be expected as the deformation of the base plate

was limited by using a thicker baseplate. In particular, the moment capacity was increased by 6% and 13% when increasing the base plate thickness from 25 to 50 and 75 mm, respectively.

Demountability of the embedded column base connections of Design 2 with various base plate thickness was studied and shown in Fig. 14(a). It is within expectation that increasing the base plate thickness achieves higher demountable bending moment (M_{de}).

Fig. 15 depicts the influences of base plate thickness on the moment capacity of the connections with various embedded lengths. It is seen that when the column was shallowly embedded ($L_e/D_{col} = 1$), the moment capacity was increased by using a thicker base plate. However, the moment capacity was less affected by the base plate thickness when the column was deeply embedded ($L_e/D_{col} = 2$).

5. Analytical model

Extensive analytical work has been conducted on the exposed bolted column-baseplate connections, many design guidelines were then produced. In contrast, analytical models for predicting the moment capacity and initial stiffness of embedded column base connections are limited. Moreover, on the basis of analysis results from above parametric studies, it can be concluded that embedded column base connections of Design 2 perform better than those of Design 1. Therefore, in the present paper, analytical

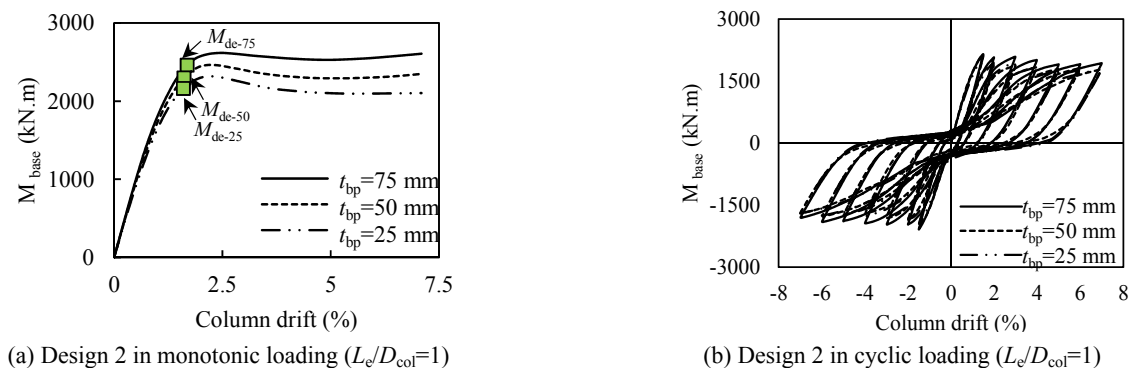


Fig. 14 Effects of base plate thickness on moment-column drift curves

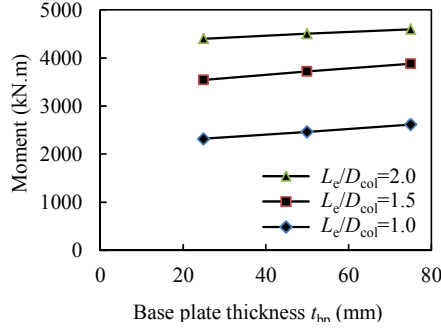


Fig. 15 Effects of base plate thickness on moment-column drift curves with different embedded lengths

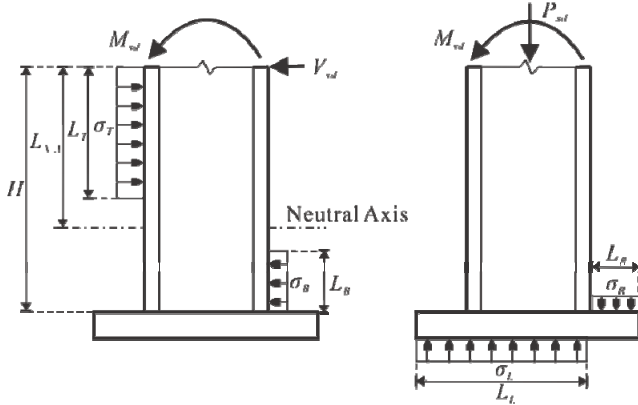


Fig. 16 Concept of analytical model for embedded column base connection

models, which can be used for design purposes, were proposed for embedded column base connections of Design 2.

5.1 Concept of the analytical model

The development of analytical models to assist the design of embedded column base connections was presented and described in this section. As illustrated in Fig. 16, a typical embedded column base connection of Design 2 was presented. The bending moment capacity and initial stiffness was assumed to be a combination of horizontal and vertical effects.

5.1.1 Bending moment capacity

In this study, the bending moment capacity of the embedded column base connection was expressed as

$$M_{j,Rd} = \alpha M_{j,H} + (1 - \alpha) M_{j,V} \quad (7)$$

where α is the distribution factor, accounting for the effective length of the embedded column. $M_{j,H}$ and $M_{j,V}$ represent the horizontal and vertical moment capacity of the connection. Specifically, the horizontal moment capacity can be expressed as

$$M_{j,H} = F_T \left(H - \frac{L_T}{2} \right) - V_{sd} H - F_B \frac{L_B}{2} \quad (8)$$

in which F_T and F_B are the resisting forces on the top and bottom flanges of the embedded column, respectively. V_{sd} is the shear force applied on top of the embedded column. The embedment length is denoted as H . L_T and L_B represent the effective length of the top and bottom contact region, respectively. In order to determine L_T and L_B , the position of neutral axis ($H_{N.A}$) should be derived by establishing horizontal equilibrium.

$$L_T = \gamma L_{N.A}; \quad L_B = \gamma (H - H_{N.A}) \quad (9)$$

$$\gamma = 0.85 - 0.007(f'_c - 28) \quad (10)$$

In Eq. (8), the resisting forces on top flanges F_T can be calculated as $F_T = \beta_T f'_c B_T L_T$, where β_T is taken as 0.85. Moreover, B_T is the effective width of the concrete resisting top compression force and is expressed as $B_T = B_f + 2c$. The determination of c is based on the finite element analysis results and can be seen through Eqs. (11)-(12). Calculation of resisting forces on bottom flanges F_B is similar, the only difference is β_B , which is taken as 0.72 to account for the embedment effects.

$$c = t_f \sqrt{\frac{f_{sy}}{f_{jd}}} \quad (11)$$

$$f_{jd} = \beta_j f'_c \sqrt{\frac{A_{c0}}{A_{c1}}} \quad (12)$$

where β_j is decided to be 0.67. A_{c1} represents the contact area of the column flange with concrete foundation and A_{c0} is the effective contact area of column flange with concrete foundation.

Vertical bending moment capacity $M_{j,V}$ was calculated from Eq. (13). D_{plate} is the depth of the base plate and L_L and L_R represent the length of the base plate subjected to compression in the left and right part of the base plate. Furthermore, F_L and F_R are the resisting forces on the base plate, which can be calculated with $F_L = \beta_v \sigma_L B_L L_L$ and $F_R = \beta_v \sigma_R B_R L_R$. In this analysis, only bearing stress failure in the left part and breakout failure of the concrete in the right part was considered. It is assumed the base plate was thick enough and consequently the failure of the base plate yielding was not involved.

$$M_{j,V} = F_L \left(D_{plate} - \frac{L_L}{2} \right) - F_R \frac{L_R}{2} \quad (13)$$

$$\sigma_L = \min \{ \sigma_{bearing}, \sigma_v^M + \sigma_v^P \} \quad (14)$$

$$\sigma_R = \min \{ \sigma_{breakout}, \sigma_v^M - \sigma_v^P \} \quad (15)$$

In Eqs. (14) and (15), bearing stress $\sigma_{bearing}$ is taken as $1.7f'_c$ to account for the confinement effect (Fisher and Kloiber 2006); breakout stress $\sigma_{breakout}$ is determined to be $6.67/(H)^{0.5}$, as proposed by Fuchs *et al.* (1995). The vertical stress induced by bending moment is determined to be $\sigma_v^M = M_{j,H}/(0.1 \times D_{plate}^2 \times B_{plate})$; while the vertical stress due to axial

Table 3 Comparison of initial stiffness and moment capacity

*Test	Axial load	Embed length	Steel column	Base plate dimension	M_{Ana}	** M_{Test} or M_{FEM}	$\frac{M_{Ana}}{M_{Test}}$	$S_{j,Ana}$	** $S_{j,Test}$ or $S_{j,FEM}$	$\frac{S_{j,Ana}}{S_{j,Test}}$
	P	L_{Emb}	-	$B_p \times D_p \times t_p$			or $\frac{M_{Ana}}{M_{FEM}}$			-
	kN	mm	-	mm	kN.m	kN.m	-	kN.m/rad	kN.m/rad	-
1	455	508	W14×370	762×762×51	2491	2580	0.97	208302	206925	0.99
2	445	508	W18×311	864×711×51	2321	2324	1.00	251302	253160	0.99
3	0	762	W14×370	762×762×51	3897	3741	1.04	211457	204318	1.03
4	455	762	W14×370	762×762×51	3924	4124	0.95	211445	213687	0.99
5	2380	455	W14×370	762×762×51	2682	2800	0.96	201279	203194	0.99
6	4760	455	W14×370	762×762×51	3168	3062	1.03	201279	204629	0.98
7	2380	680	W14×370	762×762×51	3852	3900	0.99	216316	217060	1.00
8	0	850	W18×311	864×711×51	3596	3800	0.95	254195	258271	0.98
9	1960	508	W18×311	864×711×51	2610	2550	1.02	251289	254680	0.99
10	3920	508	W18×311	864×711×51	2947	2780	1.06	251249	244060	1.03

* Tests 1-4 are experimental results from Grilli and Kanvinde (2015), Tests 5-10 are numerical analysis results from finite element modelling

** M_{Test} and $S_{i,Test}$ applied to Tests 1-4; while M_{FEM} and $S_{i,FEM}$ refer to Tests 5-10

load $\sigma_v^P = P_{sd}/(D_{plate} \times B_{plate})$ assumes a uniform stress over base plate being included according to Eqs. (14) and (15).

$$k_L = \frac{E_c \sqrt{L_L B_L}}{5.525 E_s}, \quad k_R = \frac{E_c \sqrt{L_R B_R}}{5.525 E_s} \quad (19)$$

5.1.2 Initial stiffness

For the initial stiffness prediction, the authors herein recommended a simplified approach, which comprised stiffness of the vertical and horizontal components. Initial stiffness was less affected by the axial load, which was verified by the experimental and numerical analysis results. The initial stiffness of the embedded column base connections of Design 2 can be expressed as Eq. (16)

$$S_{j,ini} = S_{j,ini-V} + (1 - \alpha) S_{j,ini-H} \quad (16)$$

in which α is the distribution factor, same as the one in Eq. (7). $S_{j,ini-V}$ and $S_{j,ini-H}$ represent the vertical and horizontal initial stiffness of the connection. Similar concepts were mentioned in Eurocode 3 (2005) and calculation of the initial stiffness can be followed per Eq. (17).

$$S_{j,ini-H} = \frac{E_s Z_H}{\left(\frac{1}{k_T} + \frac{1}{k_B}\right)}, \quad S_{j,ini-V} = \frac{E_s Z_V}{\left(\frac{1}{k_L} + \frac{1}{k_R}\right)} \quad (17)$$

where E_s is the Young's modulus of the steel column. Z_H is the distance from the centre of the top resisting force to the centre of the bottom resisting force; while Z_V represent the centre-to-centre distance of the left and right resisting forces applied on the base plate. k_T , k_B and k_L , k_R represent the stiffness of top, bottom and left and right concrete component and could be determined as

$$k_T = \frac{E_c \sqrt{L_T B_T}}{5.275 E_s}, \quad k_B = \frac{E_c \sqrt{L_B B_B}}{5.275 E_s} \quad (18)$$

In Eqs. (8) and (17), the distribution factor α play an important role in determining the moment capacity and initial stiffness. The determination of this factor largely depends on the effective embedded length ($\alpha = H_{eff}/H$). As suggested by Grilli and Kanvinde (2015), the effective length of an embedded column can be determined as

$$H_{eff} = \frac{1.77}{\left(\frac{E_c}{4E_s I_{col}}\right)^{0.25}} \quad (20)$$

in which, I_{col} represents the second moment of area of the embedded column.

5.2 Comparison of the analytical model

According to the approaches proposed in the above section, bending moment capacity and initial stiffness of a series of embedded column base connections of Design 2 are calculated and given in Table 3. The corresponding experimental and additional finite element analysis results are compared with those from the proposed analytical model.

Tests 1 to 4 were carried out by Grilli and Kanvinde (2015), where Tests 1, 2 and 4 were subjected to a combination of axial load and bending moments; while Test 3 was under pure bending. Compared with Test 1, Test 2 utilised a bigger size column and embedded in concrete foundation with the same length. Moreover, Test 4 achieved a 52% higher moment capacity than Test 1 by increasing the column embedded length to 762 mm.

Tests 5 to 10 were conducted by the authors with finite element analysis. Specifically, Tests 5 to 7 utilised the same geometric details with Test 3; the axial load and embedded length were the varied parameter. As observed in Table 3, the bending moment capacity was increased with an increase in axial load and embedded length; while the initial stiffness was only affected by the embedded length. Tests 8 to 10 utilised different column sections and investigated the effects of axial load and embedded length on the bending moment capacity and initial stiffness. Similar conclusions can be drawn.

Concluded from Table 3, the analytical model proposed by the authors not only predicts the bending moment and initial stiffness of the embedded column base connections accurately, but also matches well with the conclusions drawn from parametric studies. Moreover, the mean values of M_{Ana}/M_{Test} (M_{Ana}/M_{FEM}) and $S_{j,Ana}/S_{j,Test}$ ($S_{j,Ana}/S_{j,FEM}$) are slightly below 1.0, which means the developed analytical model can be safely used for design purposes.

6. Conclusions

Embedded steel column base connections are normally utilised in medium- to high-rise steel structures to transfer axial forces, shear forces and bending moments to the concrete foundations. Due to the significant advantages of possessing high initial stiffness, this type of column base connections is widely used in seismic-prone regions. In the present paper, the proposed finite element model can accurately predict the behaviour of embedded steel column base connections in terms of initial stiffness and bending moment strength similar to the experimental results.

Comparisons between finite element models and experimental results from the literature showed that the failure modes, initial stiffness and bending moment capacities obtained from the finite element model agree well with the experiments. The validated finite element model was further extended to conduct parametric studies on different types of embedded steel column base connections under monotonic and cyclic loading. The effects of four parameters were investigated through finite element analysis by varying one parameter each time.

According to the finite element analysis results of parametric and demountability studies, the authors concluded that an increase in axial load generally increases the initial stiffness, bending moment capacity and demountability of the embedded column base connections. However, the behaviour of the embedded column base connections would be negatively affected when the axial loads exceeded 40% P_{des} due to the occurrence of local buckling in the steel column. Concrete compressive strength and base plate thickness played an important role in improving the behaviour of the embedded column base connections. Normally, increasing concrete compressive strength or base plate thickness increases the bending moment capacity and demountability of the connections. Nevertheless, the initial stiffness was less affected by the base plate thickness. As one of the most critical parameters, embedded length significantly influences the performance of the embedded column base connections. Furthermore,

the effects of other parameters are somehow affected by varying the steel column embedded length. Generally, increasing the column embedded length can increase the initial stiffness, bending moment capacity and demountability of the embedded column base connections. In addition, the increase in column embedded length can reduce the effects of other parameters, such as axial load and base plate thickness.

For the design purposes, this paper also proposed an analytical model for a certain type of embedded column base connection. Compared with the experimental results and finite element analysis results, it was found that the proposed analytical model can accurately predict the initial stiffness and moment capacity of the embedded column base connections. Moreover, due to the mean values of M_{Ana}/M_{Test} (M_{Ana}/M_{FEM}) and $S_{j,Ana}/S_{j,Test}$ ($S_{j,Ana}/S_{j,FEM}$) being slightly below 1.0, the proposed model is conservative and safe in design use.

Acknowledgments

The research described in this paper is financially supported by the Australian Research Council (ARC) under its Discovery Scheme (Project No: DP140102134). The financial support is gratefully acknowledged.

References

- ABAQUS (2012), Analysis User's Manual, ABAQUS Standard, Version 6.12.
- ACI-318 (2008), Building code requirements for reinforced concrete, ACI, Detroit, MI, USA.
- Ali, A., Kim, D. and Cho, S.G. (2013), "Modelling of nonlinear cyclic load behaviour of I-shaped composite steel-concrete shear walls of nuclear power plants", *Nucl. Eng. Technol.*, **45**(1), 89-98.
- Aslani, F., Uy, B., Tao, Z. and Mashiri, F. (2015), "Behaviour and design of composite columns incorporating compact high-strength steel plates", *J. Constr. Steel Res.*, **107**, 94-110.
- Birtel, V. and Mark, P. (2006), "Parameterised finite element modelling of RC beam shear failure", ABAQUS Users' Conference, pp. 95-108.
- Carreira, D. and Chu, K. (1985), "Stress-strain relationship for plain concrete in compression", *Amer. Conc. I.*, **82**(6), 797-804.
- Chaboche, J.L. (1994), "Modelling of ratchetting: evaluation of various approaches", *Eur. J. Mech., A/Solids*, **13**, 501-518.
- Clark, P., Frank, K., Krawinkler, H. and Shaw, R. (1997), "Protocol for fabrication, inspection, testing, and documentation of beam-column connection tests and other experimental specimens", SAC Steel Project Background Document; Report No. SAC/BD-97/02, October.
- Cui, Y., Nagae, T. and Nakasima, M. (2009), "Hysteretic behaviour and strength capacity of shallowly embedded steel column bases", *J. Struct. Eng.-ASCE*, **135**(10), 1231-1238.
- Demir, S., Husem, M. and Pul, S. (2014), "Failure analysis of steel column-RC base connections under lateral cyclic loading", *Struct. Eng. Mech., Int. J.*, **50**(4), 459-469.
- Eurocode 3, Part 1-8 (2005), Design of steel structures – Design of joints, European Committee for Standardisation; Brussel, Belgium.
- Fisher, J.M. and Kloiber, L.A. (2006), "Base plate and anchor rod design", (2nd Ed.), Steel Design Guide Series No. 1, American Institute of Steel Construction, Inc., Chicago, IL, USA.

- Fuchs, W., Eligehausen, R. and Breen, J.E. (1995), "Concrete capacity design approach for fastening to concrete", *ACI Struct. J.*, **92**(1), 73-94.
- Grauvilardell, J.E., Lee, D., Hajjar, J.F. and Dexter, R.J. (2005), "Synthesis of design, testing and analysis research on steel column base plate connections in high seismic zones", *Structural Engineering*, Rep. No. ST-04-02; Department of Civil Engineering, University of Minnesota, Minneapolis, MN, USA.
- Green Building Council of Australia (2009), *Green Star Overview*. URL: www.gbca.org.au
- Grilli, D.A. and Kanvinde, A.M. (2015), "Embedded column base connections subjected to flexure and axial load: Tests and strength models", Final report presented to the American Institute of Steel Construction, Chicago, IL, USA.
- Heristchian, M., Pourakbar, P., Imeni, S. and Ramezani, R.A. (2014), "Ultimate tensile strength of embedded I-sections: a comparison of experimental and numerical results", *Int. J. Adv. Struct. Eng.*, **6**, 169-180.
- Jia, L.J. and Kuwamura, H. (2014), "Prediction of cyclic behaviours of mild steel at large plastic strain using coupon tests results", *J. Struct. Eng.-ASCE*, **140**(2), 441-454.
- Koch, E., Mang, F., Schleich, J.B., Seiler, J. and Stiglat, K. (1993), "Steel columns embedded in concrete foundation", *Proceedings of the 4th International Conference on Structural Failure, Durability and Retrofitting*, Singapore, September.
- Lorenz, E. and Vangeem, M.G. (2011), "Designing green", *Modern Steel Construction*, May.
- Mirza, O. and Uy, B. (2011), "Behaviour of composite beam-column flush end-plate connections subjected to low-probability, high-consequence loading", *Eng. Struct.*, **33**(2), 647-662.
- Pertold, J., Xiao, R.Y. and Wald, F. (2000), "Embedded steel column bases – I. Experimental and numerical simulation", *J. Constr. Steel Res.*, **56**, 253-270.
- Silvestre, E., Mendiguren, J., Galdos, L. and Argandoña, E. (2015), "Comparison of the hardening behaviour of different steel families: from mild and stainless steel to advanced high strength steels", *Int. J. Mech. Sci.*, **101-102**, 10-20.
- Thai, H.T. and Uy, B. (2015), "Finite element modelling of blind bolted composite joints", *J. Constr. Steel Res.*, **112**, 339-353.
- Uy, B. (2014), "Innovative connections for the demountability and rehabilitation of steel", *Space and Composite Structures*, Prague, Czech Republic.
- Uy, B., Patel, V.I. and Li, D. (2015), "Behaviour and design of connections for demountable steel and composite structures", *Proceedings of the 11th International Conference on Advances in Steel and Concrete Composite Structures*, Beijing, China, December.
- Uy, B., Patel, V.I., Li, D. and Aslani, F. (2016), "Behaviour and design of connections for demountable steel and composite structures", *Structures*, DOI: 10.1016/j.istruc.2016.06.005
- Winters-Downey, E. (2010), "Reclaimed structural steel and LEED Credit MR-3 – Materials Reuse", *Modern Steel Construction*, May.